PADOVA UNIVERSITY PRESS

Dolomites Research Notes on Approximation

Special Issue dedicated to Robert Schaback on the occasion of his 75th birthday, Volume 15 · 2022 · Pages 37–48

# Reconstruction of volatility surfaces: a first computational study

Salvatore Cuomo[a] · Alessandra De Rossi[b] · Luca Rizzo[b,c] · Federica Sica[a]

*Communicated by Francesco Marchetti*

**Abstract**

Option prices are usually represented by a three-dimensional set of volatility values, implied by the Black-Scholes formula or a stochastic model like the Heston model. Given such volatility points, it is required to reconstruct the corresponding volatility surface via an interpolation method. From the point of view of interpolation, it is intriguing to work with a particular data-set such as the one shown in the current work. This set is characterized by unscattered or non-specifically distributed data: they are rather arranged along lines. In this paper, we present a computational study based on radial basis function (RBF) methods. Initially, a reconstruction of the surface has been made globally, then the obtained output has been tested by removing points and evaluating errors. Furthermore, local methods such as RBF-partition of unity method have been adopted with variable sizes of subdomains and shape parameters. To improve the interpolant accuracy we propose a strategy consisting in adding points which were computed through the least square method. One of the issues of the financial world is to extrapolate the option volatility surface for unknown tenors and strikes, and therefore the study further develops these methods in order to cover extrapolated regions.

## Introduction

The **Black-Scholes-Merton** (BS) model was originally conceived in 1969, but it was later published with its derivation in 1973 [2]. The model consists of a linear parabolic partial differential equation (PDE) which defines the behavior of a financial product, whose value $V(S(t),t)$ depends on an asset $S(t)$ and, naturally, on time $t$. We will refer to $S(t)$ as the *underlying*, and it may represent a stock, a forward rate, or another asset price.

The main hypothesis of the model consists in assuming $S(t)$ be a Geometric Brownian motion (GBM), i.e. $S(t)$ is lognormally distributed. Formally:

$$dS = \mu S dt + \sigma S dW, \tag{1}$$

where $\mu$ is the *drift*, $\sigma$ the *volatility* of the asset and $W$ a Brownian motion. Following [2], we can derive the BS partial differential equation:

$$\frac{\partial V}{\partial t} + \frac{1}{2}\sigma^2 S^2 \frac{\partial^2 V}{\partial S^2} + rS\frac{\partial V}{\partial S} - rV = 0. \tag{2}$$

BS model assumes a constant or time-dependent volatility $\sigma(t)$. Since the model also provides an analytical formula for the price of simple derivatives, it is natural to try to derive the volatility of the underlying $S(t)$ by inverting the given formula. Such volatility is called **implied volatility**, and can be interpreted as the expected value of the future volatility by market participants. By simply plotting the values corresponding to the same type of contract with various parameters, traders observed the well-known shape of a **volatility smile**: volatility is actually not constant but varies with the derivative's $V(S(t),t)$ parameters.

In order to capture a specific behavior of the volatility, called volatility smile, research has enriched the Black-Scholes model by modeling the volatility as a function of both underlying asset and time: the most known attempt is the **local volatility model** by Dupire, Derman and Kani ([12], [11], [13]). Such a model is easy to calibrate and guarantees a perfect and complete market.

A further extension consists in considering a **stochastic volatility**, which exhibits an intrinsic source of randomness given by a Brownian motion. The **Heston model** [19] or **SABR** model [18] are stochastic volatility models which consider a more realistic asset distribution than the original, lognormal distribution of the BS framework. Furthermore, they both provide a semi-analytical solution for European options: this result is extremely useful for the calibration of the model itself. By choosing a stochastic model, the volatility is directly modeled and market expectations are imposed as model constraints in order to obtain the desired volatility smile.

In the real world, a trader makes use of the numerical or analytical derivatives of an option price to its risk factors - e.g. the option volatility - in order to be able to hedge the transactions in her portfolio. In practice, such derivatives represent the risks

[a] Department of Mathematics and Application "R. Caccioppoli", University of Naples Federico II, Via Cintia, Naples, Italy

[b] Department of Mathematics “G. Peano”, University of Turin, via Carlo Alberto 10, Turin, Italy

[c] Collegio Carlo Alberto, Piazza Arbarello 8, Turin, Italy

the trader's portfolio is exposed to: if the volatility value changes, the price of the option will change accordingly and it will have an impact on the portfolio profit and loss (PnL) measure. By choosing an interpolation that guarantees arbitrage-free properties, the option prices and the related risks will be more in line with the theory and hence more accurate.
The main purpose of this paper is to investigate the potential efficiency and accuracy of the implied volatility surface interpolation via **radial basis function** (RBF) methods.

Meshfree methods are popular tools for solving problems of interpolation, integration and numerical resolution of differential equations. They take advantage of being flexible with respect to the geometry of the problem, are easy to implement in higher dimensions, and can also provide high order convergence. The RBF method is a meshless method very accurate and effective (see e.g. [3, 6, 14, 15, 20, 27]). The main disadvantage of radial kernel method is the computational cost associated with the solution of the linear system. Moreover, the interpolant is global, i. e. it is constructed using all the nodes of the dataset. Therefore, a change in the nodes influences the entire interpolation result. For these reasons, in the last decade research has been directed towards considering local methods involving RBFs. Recently, in approximation theory a specific method has been proved to be effective for interpolation of large scattered data sets, the Partition of Unity Method (PUM) (see e.g. [7, 8, 14, 26]). Its origin can be found in the context of partial differential equations (PDEs) [1, 21]. In scattered data interpolation, PUM is implemented using RBFs as local approximants, since this is the most efficient tool for interpolation of scattered data [14].

In this paper, since the RBF and partition of unity methods were already used in financial applications and in particular in volatility analysis (see e.g. [9, 10, 22, 24, 25]), the two methods are considered for implied volatility surface interpolation. We performed an extensive experimentation using a dataset obtained by the Bloomberg platform, where the quoted points consist of implied volatilities of options with the Apple's stock as underlying. The experiments show good results using the two methods and the computational study suggests that new and promising investigations are required especially for the extrapolation of the volatility surface.

The paper is organized as follows. In Section 1 we introduce some financial preliminaries. In Sections 2 the radial basis function method and the partition of unity method are presented, in particular the interpolation of volatility surfaces using RBF is considered. Section 3 is devoted to the presentation of numerical experiments and the computational study. Finally, Section 4 deals with conclusions and future work.

## 1 Financial preliminaries

In financial applications it is well-known that a Black-Scholes (BS) solution of a pricing problem depends on the type of contract $V(S(t), t)$ we aim to price. Each contract yields a different terminal condition which will impact the analytical expression of the corresponding solution. In case $V(t)$ represents a vanilla product, the Black-Scholes PDE provides an analytical solution. An example of a vanilla product is a *European option*: a **European call** (respectively **put**) option on the amount of $S$ units of currency, with **strike price** K and **exercise date** T, is a contract written at $t = 0$ with the following property: the holder of the contract has, **exactly at the time** $t = T$, the right but not the obligation to buy (respectively sell) $S$ at the price $K$.

The adjective *European* defines the time at which the option can be exercised, i.e. the holder can decide to sell or buy the underlying at price K. The adjectives *call* or *put* simply define if the holder can buy or sell the underlying. The option expires on a date $T$, which denotes the *maturity* of the contract. After such date, the option cannot be exercised anymore and loses any value. In order to price options, we require additional information regarding the initial and boundary conditions of the BS PDE (2). Since the BS is typically solved backwards in time, we will refer to the initial condition as the *terminal condition* at time $t = T$.

$$V(S,T) = \phi(S,T) := max(S(T) - K, 0) \qquad \text{for a call} \tag{3}$$
$$V(S,T) = \phi(S,T) := max(K - S(T), 0) \qquad \text{for a put.} \tag{4}$$

Therefore, the terminal condition is defined by the payoff function $\phi$. The boundary conditions associated to the PDE for European options are:

**Boundary Conditions for European Call Options**

$$V(S,t) = 0 \quad \text{as} \quad S \to 0 \tag{5}$$
$$V(S,t) = S \quad \text{as} \quad S \to +\infty. \tag{6}$$

**Boundary Conditions for European Put Options**

$$V(S,t) = Ke^{-r(T-t)} \quad \text{as} \quad S \to 0 \tag{7}$$
$$V(S,t) = 0 \qquad \text{as} \quad S \to +\infty. \tag{8}$$

Given terminal and boundary conditions, the BS analytical formulae for European call and put options become:

$$V_{call}(S,t) = SN(d_1) - Ke^{-r(T-t)}N(d_2) \tag{9}$$
$$V_{put}(S,t) = Ke^{-r(T-t)}N(-d_2) - SN(-d_1)$$

where $N(\cdot)$ is the cumulative normal distribution and:

$$d_1 := \frac{\log\left(\frac{S}{K}\right) + r + \frac{1}{2}\sigma^2(T-t)}{\sigma\sqrt{T-t}} \tag{10}$$
$$d_2 := d_1 - \sigma\sqrt{T-t} \tag{11}$$

More flavors of options are available in the market - for example American options, which allow buying or selling the asset at any time earlier than the expiry date - and it is possible to model extra features by extending the BS PDE, but the complexity of the problem increases and it is not possible anymore to derive an analytical solution.
In option markets, it is common to express the price of an option in terms of its **implied volatility**. We can define the implied volatility of an option with price $V(S,t)$ with strike $K$ and expiry $T$ as the time-dependent function $\sigma_{IV}^{K,T}(S,t)$ as the solution to problem (9). We define the $T^\star$**-maturity volatility smile** as the mapping $K \longmapsto \sigma_{IV}^{K,T^\star}$ for a fixed maturity $T^\star$. Several volatility smiles for different $T$ form a so-called **volatility surface**, described by the mapping $(K,T) \longmapsto \sigma_{IV}^{K,T}$.

In general, solving (9) for $\sigma_{IV}^{K,T}(S,t)$ represents an inverse problem and is usually solved with a Newton-Raphson or Brent's algorithm. Newton-Raphson's method is more efficient and convenient to use in case of European options, since the derivative of the price with respect to the volatility - a quantity required to find the root - is available via an analytical formula. Implied volatilities are usually quoted in the market, and traders trade options in terms of volatility instead of prices.
Since only a finite set of $\sigma_{IV}$ for options with maturity $T$ and strike $K$ are quoted in the market, it is necessary to interpolate the quoted implied volatilities for the missing $(K,T)$. The chosen interpolation method must fit the initial points and provide a smooth volatility surface: according to arbitrage-free theory, a volatility surface is free of static arbitrage if and only if it is free of calendar spread arbitrage and each time slice is free of butterfly arbitrage [17].

## 2 Approximation methods

In the following, we first recall some preliminaries on RFB interpolation and then we discuss the partition of unity approximation scheme. Finally, we introduce the interpolation of volatility surface problem by means of RBF.

### 2.1 RBF interpolation

Given a set $\mathcal{X}_N = \{\boldsymbol{x}_i \in \mathbb{R}^M, i = 1,\ldots,N\}$ of $N$ distinct *data points*, also called *data sites* or *nodes*, in a domain $\Omega \subseteq \mathbb{R}^M$, and a corresponding set $\mathcal{F}_N = \{f_i = f(\boldsymbol{x}_i), i = 1,\ldots,N\}$ of *data values* or *function values* obtained by possibly sampling any (unknown) function $f : \Omega \longrightarrow \mathbb{R}$, the standard RBF interpolation problem consists in finding an interpolant $R : \Omega \longrightarrow \mathbb{R}$ of the form

$$R(\boldsymbol{x}) = \sum_{i=1}^{N} c_i \phi(||\boldsymbol{x} - \boldsymbol{x}_i||_2), \quad \boldsymbol{x} \in \Omega, \tag{12}$$

where $||\cdot||_2$ is the Euclidean norm, and $\phi : [0,\infty) \longrightarrow \mathbb{R}$ is a RBF [3, 20]. The coefficients $\{c_i\}_{i=1}^N$ are determined by enforcing the interpolation conditions

$$R(\boldsymbol{x}_i) = f_i, \quad i = 1,\ldots,N. \tag{13}$$

Imposing the conditions (13) leads to a symmetric linear system of equations

$$\Phi \boldsymbol{c} = \boldsymbol{f}, \tag{14}$$

where $\Phi_{ki} = \phi(||\boldsymbol{x}_k - \boldsymbol{x}_i||_2)$, $k,i = 1,\ldots,N$, $\boldsymbol{c} = [c_1,\ldots,c_N]^T$, and $\boldsymbol{f} = [f_1,\ldots,f_N]^T$. When $\boldsymbol{c}$ is found by solving the system (14), we can evaluate the RBF interpolant at a point $\boldsymbol{x}$ as

$$R(\boldsymbol{x}) = \boldsymbol{\phi}^T(\boldsymbol{x})\boldsymbol{c},$$

where $\boldsymbol{\phi}^T(\boldsymbol{x}) = [\phi(||\boldsymbol{x} - \boldsymbol{x}_1||_2),\ldots,\phi(||\boldsymbol{x} - \boldsymbol{x}_N||_2)]$.
The interpolation problem is well-posed, i.e. a solution to the problem exists uniquely, if and only if the matrix $\Phi$ is nonsingular. A sufficient condition to have nonsingularity is that $\Phi$ is positive definite. Thus, if the matrix $\Phi$ is positive definite, then all its eigenvalues are positive and $\Phi$ is nonsingular. Therefore, the function $\phi$ is strictly positive definite, and consequently the interpolant (12) is unique [14]. In Table 1 we report a list of some strictly positive definite RBFs with their smoothness degrees. In particular, we remark that Gaussian, Inverse MultiQuadric, Inverse Quadratic and Matérn functions are globally supported and strictly positive definite in $\mathbb{R}^M$ for any $M$, whereas Wendland functions are compactly supported – with support $[0,1/\varepsilon]$ – and strictly positive definite in $\mathbb{R}^M$ for $M \leq 3$ (see [16, 27]).

| RBF | $\phi_\varepsilon(r)$ |
|---|---|
| Gaussian $C^\infty$ (GA) | $\mathrm{e}^{-\varepsilon^2 r^2}$ |
| MultiQuadric $C^\infty$ (MQ) | $(1+\varepsilon^2 r^2)^{1/2}$ |
| Inverse MultiQuadric $C^\infty$ (IMQ) | $(1+\varepsilon^2 r^2)^{-1/2}$ |
| Inverse Quadric $C^\infty$ (IQ) | $(1+\varepsilon^2 r^2)^{-1}$ |
| Thin Plate Spline $C^\infty$ (TPS) | $r^2 \log r$ |
| Matérn $C^6$ (M6) | $\mathrm{e}^{-\varepsilon r}(\varepsilon^3 r^3 + 6\varepsilon^2 r^2 + 15\varepsilon r + 15)$ |
| Matérn $C^4$ (M4) | $\mathrm{e}^{-\varepsilon r}(\varepsilon^2 r^2 + 3\varepsilon r + 3)$ |
| Matérn $C^2$ (M2) | $\mathrm{e}^{-\varepsilon r}(\varepsilon r + 1)$ |
| Wendland $C^6$ (W6) | $(1-\varepsilon r)_+^8 (32\varepsilon^3 r^3 + 25\varepsilon^2 r^2 + 8\varepsilon r + 1)$ |
| Wendland $C^4$ (W4) | $(1-\varepsilon r)_+^6 (35\varepsilon^2 r^2 + 18\varepsilon r + 3)$ |
| Wendland $C^2$ (W2) | $(1-\varepsilon r)_+^4 (4\varepsilon r + 1)$ |

**Table 1:** Examples of RBFs with their orders of smoothness and shape parameter $\varepsilon > 0$; $r = ||\cdot||_2$ is the Euclidean norm and $(\cdot)_+$ denotes the truncated power function.

### 2.2 Partition of unity approximation

Let $\Omega \subseteq \mathbb{R}^M$ be an open and bounded domain, and let $\{\Omega_j\}_{j=1}^d$ be an open and bounded covering of $\Omega$ satisfying some mild overlap condition among the subdomains $\Omega_j$, i.e. the overlap among the subdomains must be sufficient so that each interior point $\boldsymbol{x} \in \Omega$ is located in the interior of at least one subdomain $\Omega_j$. The set $I(\boldsymbol{x}) = \{j : \boldsymbol{x} \in \Omega_j\}$, for $\boldsymbol{x} \in \Omega$, is uniformly bounded on $\Omega$, with $\Omega \subseteq \bigcup_{j=1}^d \Omega_j$.

Associated with the subdomains we choose partition of unity weight functions $W_j$, i.e. a family of compactly supported, nonnegative and continuous functions subordinate to the subdomain $\Omega_j$, such that $\sum_{j=1}^d W_j(\boldsymbol{x}) = 1$ on $\Omega$ and $\mathrm{supp}(W_j) \subseteq \Omega_j$. The global approximant is thus constructed as follows

$$\mathcal{I}(\boldsymbol{x}) = \sum_{j=1}^{d} R_j(\boldsymbol{x}) W_j(\boldsymbol{x}), \quad \boldsymbol{x} \in \Omega, \tag{15}$$

where $R_j$ defines a local RBF interpolant on each subdomain $\Omega_j$ and $W_j : \Omega_j \longrightarrow \mathbb{R}$ is a partition of unity weight function.

According to [26], we assume to have a $k$-stable partition of unity, i.e a family of nonnegative functions $\{W_j\}_{j=1}^d$, with $W_j \in C^k(\mathbb{R}^M)$, such that:

i. $\mathrm{supp}(W_j) \subseteq \Omega_j$,

ii. $\sum_{j=1}^d W_j(\boldsymbol{x}) = 1$ on $\Omega$,

iii. $||D^\beta W_j||_{L^\infty(\Omega_j)} \le \frac{C_\beta}{\delta_j^{|\beta|}}$, $\forall \beta \in \mathbb{N}^M : |\beta| \le k$, where $\delta_j$ is the diameter of $\Omega_j$ and $C_\beta > 0$ is a constant.

As nonnegative functions $W_j \in C^k(\mathbb{R}^M)$, we consider Shepard's weight, i.e.,

$$W_j(\boldsymbol{x}) = \frac{\varphi_j(\boldsymbol{x})}{\sum_{k \in I(\boldsymbol{x})} \varphi_k(\boldsymbol{x})}, \quad j = 1, \ldots, d,$$

$\varphi_j(\boldsymbol{x})$ being compactly supported functions with support on $\Omega_j$ such as Wendland's functions [27].

*Remark* 1. If the functions $R_j$, $j = 1, \ldots, d$, satisfy the interpolation conditions $R_j(\boldsymbol{x}_i) = f(\boldsymbol{x}_i)$ for each $\boldsymbol{x}_i \in \Omega_j$, then the global partition of unity approximant inherits the interpolation property of the local interpolants [14], i.e.

$$\mathcal{I}(\boldsymbol{x}_i) = \sum_{j=1}^{d} R_j(\boldsymbol{x}_i) W_j(\boldsymbol{x}_i) = \sum_{j \in I(\boldsymbol{x}_i)} f(\boldsymbol{x}_i) W_j(\boldsymbol{x}_i) = f(\boldsymbol{x}_i).$$

In order to be able to formulate error bounds, we need some further assumptions on regularity of $\Omega_j$ and define the *fill distance*

$$h_{\mathcal{X}_N,\Omega} = \sup_{\boldsymbol{x} \in \Omega} \min_{\boldsymbol{x}_i \in \mathcal{X}_N} ||\boldsymbol{x} - \boldsymbol{x}_i||_2. \tag{16}$$

Specifically, we require that an open and bounded covering $\{\Omega_j\}_{j=1}^d$ is *regular* for $(\Omega, \mathcal{X}_N)$. This means to fulfill the following properties [26]:

i. for each $\boldsymbol{x} \in \Omega$, the number of subdomains $\Omega_j$ with $\boldsymbol{x} \in \Omega_j$ is bounded by a global constant $C$;

ii. there exists a constant $C_r > 0$ and an angle $\theta \in (0, \pi/2)$ such that every subdomain $\Omega_j$ satisfies an interior cone condition with angle $\theta$ and radius $r = C_r h_{\mathcal{X}_N,\Omega}$;

iii. the local fill distances $h_{\mathcal{X}_{N_j},\Omega_j}$ are uniformly bounded by the global fill distance $h_{\mathcal{X}_N,\Omega}$, where $\mathcal{X}_{N_j} = \mathcal{X}_N \cap \Omega_j$.

*Remark* 2. The assumptions above lead to the requirement that the number of subdomains is proportional to the number of data [27]. The first property ensures that (15) is actually a sum over at most $C$ summands. Moreover, it is crucial for an efficient evaluation of the global approximant that only a constant number of local interpolants be evaluated. It follows that it should be possible to locate those $C$ indices in constant time. The second and third properties are significant for estimating errors of RBF interpolants.

After defining the space $C_\nu^k(\mathbb{R}^M)$ of all functions $f \in C^k$ whose derivatives of order $|\beta| = k$ satisfy $D^\beta f(\boldsymbol{x}) = \mathcal{O}(||\boldsymbol{x}||_2^\nu)$ for $||\boldsymbol{x}||_2 \longrightarrow 0$, we consider the following convergence result [14, 27].

**Theorem 2.1.** *Let $\Omega \subseteq \mathbb{R}^M$ be an open and bounded domain and suppose that $\mathcal{X}_N = \{\boldsymbol{x}_i, i = 1, \dots, N\} \subseteq \Omega$. Let $\phi \in C_\nu^k(\mathbb{R}^M)$ be a strictly positive definite function. Let $\{\Omega_j\}_{j=1}^d$ be a regular covering for $(\Omega, \mathcal{X}_N)$ and let $\{W_j\}_{j=1}^d$ be k-stable for $\{\Omega_j\}_{j=1}^d$. Then the error between $f \in \mathcal{N}_\phi(\Omega)$, where $\mathcal{N}_\phi = span\{\phi(||\boldsymbol{x} - \cdot||_2), \boldsymbol{x} \in \Omega\}$, is the native space of $\phi$, and its partition of unity interpolant* (15) *can be bounded by:*

$$|D^\beta f(\boldsymbol{x}) - D^\beta \mathcal{I}(\boldsymbol{x})| \leq C' h_{\mathcal{X}_N,\Omega}^{\frac{k+\nu}{2}-|\beta|} |f|_{\mathcal{N}_\phi(\Omega)},$$

*for all $\boldsymbol{x} \in \Omega$ and all $|\beta| \leq k/2$, where $C'$ is a constant independent of $\boldsymbol{x}$, $f$ and $\phi$.*

*Remark* 3. If we compare the result reported in Theorem 2.1 with the global error estimates shown in [27], we can see that the partition of unity interpolant preserves the local approximation order for the global fit. Thus, the partition of unity approach enables us to decompose a large problem into many small ones and, at the same time, ensures that the accuracy obtained for the local fits is carried over to the global interpolant.

*Remark* 4. From Theorem 2.1, we can note that the interpolation error decreases together with the fill distance. Anyway, consistently with the trade-off or uncertainty *principle* [23], a conflict between theoretical accuracy and numerical stability may occur. In fact, if a large number of interpolation nodes is involved, the local RBF systems may suffer from ill-conditioning. The latter is linked to the order of the basis functions and to the node distribution. Therefore, the ill-conditioning grows if the fill distance decreases. In such case, in order to avoid numerical problems, for high density of interpolation points, we can use low-order basis functions or Compactly Supported RBFs (CSRBFs) [14]. However, more recently several approximation techniques have been proposed in order to obtain a stable computation with flat RBFs [16] or a stable basis to be used [4].

### 2.3 Interpolation of volatility surfaces using RBF

Since RBF are mainly used as an interpolation method, it is simply natural to apply such method to reconstruct a volatility surface. Given initial market data points, consisting in implied volatilities $\sigma(K, T)$ associated to the corresponding option with Black-Scholes price, we can interpolate said points and imply a volatility value for missing market data.

Formally, given a grid of strikes times maturities of the respective options, i.e. $[K \times T]$, with known points $\sigma(K_i, T_j)$ $\forall (K_i, T_j) \in \{K_1, \dots, K_n\} \cdot \{T_1, \dots, T_m\}$, where $m, n \in \mathbb{N}$, we aim to find values of $\sigma(K_l, T_h)$ where $l \notin \{1, \dots, n\}$ and $h \notin \{1, \dots, m\}$. For the sake of simplicity, if we define $\mathbf{x} := (K, T) \in \mathbb{R}^2$ we are required to solve the following scattered data problem in $\mathbb{R}^2$:

$$\hat{\sigma}(\mathbf{x}) = \sum_{k=1}^{N} c_k \phi(||\mathbf{x} - \mathbf{x}_k||_2) \tag{17}$$

where $\hat{\sigma}(\mathbf{x})$ is the approximation of the volatility function we want to recover; $\phi$ the chosen radial basis function; $c_k \in \mathbb{R}$ are the coefficients we need to find in order to calculate the linear approximation of the volatility function given above; and $\mathbf{x}_k \in \mathbb{R}^2$ are the chosen centers. Equation (17) is a straightforward adaptation of the RBF theory. Hence, in order to obtain the coefficient $c_k$ and compute the volatility function we need to solve the following system:

$$\begin{bmatrix} \phi(||\mathbf{x}_1 - \mathbf{x}_1||_2) & \dots & \phi(||\mathbf{x}_1 - \mathbf{x}_N||_2) \\ \phi(||\mathbf{x}_2 - \mathbf{x}_1||_2) & \dots & \phi(||\mathbf{x}_2 - \mathbf{x}_N||_2) \\ \dots & \dots & \dots \\ \phi(||\mathbf{x}_N - \mathbf{x}_1||_2) & \dots & \phi(||\mathbf{x}_N - \mathbf{x}_N||_2) \end{bmatrix} \begin{bmatrix} c_1 \\ c_2 \\ \dots \\ c_N \end{bmatrix} = \begin{bmatrix} \sigma(\mathbf{x}_1) \\ \sigma(\mathbf{x}_2) \\ \dots \\ \sigma(\mathbf{x}_N) \end{bmatrix}. \tag{18}$$

## 3 Numerical experiments

In order to reconstruct the volatility surface, we begin with exploiting global methods based on radial basis functions. Global interpolation has been performed using different radial basis functions in order to take advantage of their several characteristics and to find out the best way to reconstruct the surface. Later, surfaces are tested by using cross validation to check how the interpolation performs globally and also in the regions with low points density. In order to test the accuracy of the proposed methods, we used the cross validation approach by:

- computing the results with several kernels and orders of smoothness,

- calculating the corresponding Maximum Absolute Error (MAE) and the Root Mean Square Error (RMSE).

The formulae for (MAE) and (RMSE) are respectively given by:

$$MAE = \max_{1\leq i\leq s} |f(\tilde{x}_i, \tilde{y}_i) - \mathcal{I}(\tilde{x}_i, \tilde{y}_i)|, \qquad RMSE = \sqrt{\frac{1}{s}\sum_{i=1}^{s} |f(\tilde{x}_i, \tilde{y}_i) - \mathcal{I}(\tilde{x}_i, \tilde{y}_i)|^2}.$$

where $\mathcal{I}$ denotes the interpolant and $f$ the exact function.

At a later stage, we opt for a more local approach such as the partition of unity method in order to improve the fitting grade in the steepest regions. Eventually, we choose to extrapolate the surface in the time direction starting with a globally interpolated surface.

### 3.1 Numerical tests using RBF global interpolation

The points of the dataset are obtained by Bloomberg's platform and they consists of the values of implied volatilities of options with the Apple's stock as underlying. In the following, we will refer to implied volatility as $\sigma(K, T)$, where $K$ is the strike price of the option and $T$ is its expiry date. The dataset used, and below described, consists of 144 data and we consider as evaluation date 29/01/2021. The sixteen time steps are not constant: while the firsts steps are about one week, the following ones become larger. The given strike prices vary from 80% and 120% of the price on the valuation date that is 132.82 US dollars. In this direction we find two quite big strips without data points: this characteristic will become important when we will use the method of partition of unity. Below in Figure 1 the volatility's dataset is shown.

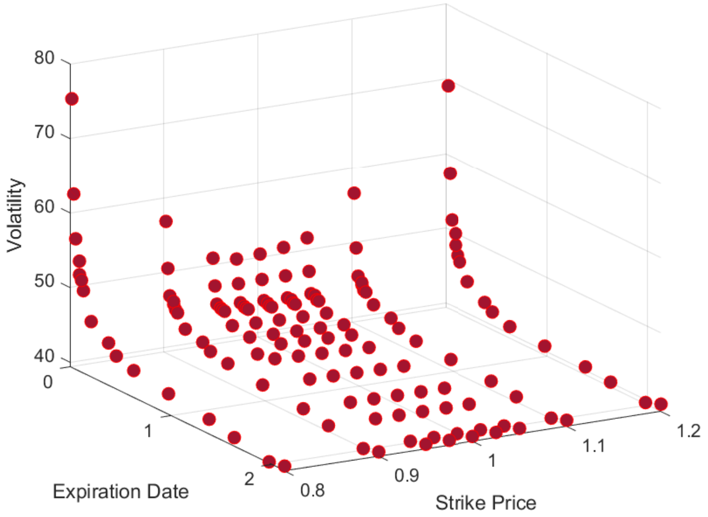

**Figure 1:** The set of 144 volatility's points.

In Figure 1 implied volatility values are shown on the vertical axis, while on the left axis we represent the expiration dates converted in years, and on the remaining axis strike prices are represented. The reconstruction of surfaces methods based on radial basis functions are typically used on scattered data. Instead, our points distribution is very unusual for these methods since the data are arranged along lines, so it is quite intriguing to study such a dataset from a numerical point of view. The dataset shows two different regions: the first one - relatively steep - which contains the greater number of points and the second one, flat, with more spaced points. Moreover, there are two bands characterized by a low data density corresponding at the intervals with strike prices ranging between 80% - 90% and 110% - 120%.

At first the surface reconstruction has been performed by using a global interpolant method based on radial basis functions. Several RBF types (e.g. Gaussian, Thin Plate Spline, Multiquadric, Inverse Multiquadric) have been used, trying to better exploit their different shapes. The best results are obtained by using Thin Plate Spine and Multiquadric with a shape parameter of $\epsilon = 110$. Results are shown in Figure 2 and Figure 3.

The main differences between the obtained interpolants are due to the different properties of the chosen base functions. For instance, radial functions like Gaussian do not perform very well due to their flat zones approach to zero away from the function's center. Differently, the Thin Plate Spline, which normally provides smooth surfaces, produces accurate interpolants, an example is shown in the figure below. Similar results can be obtained with other radial basis functions such as Multiquadric.

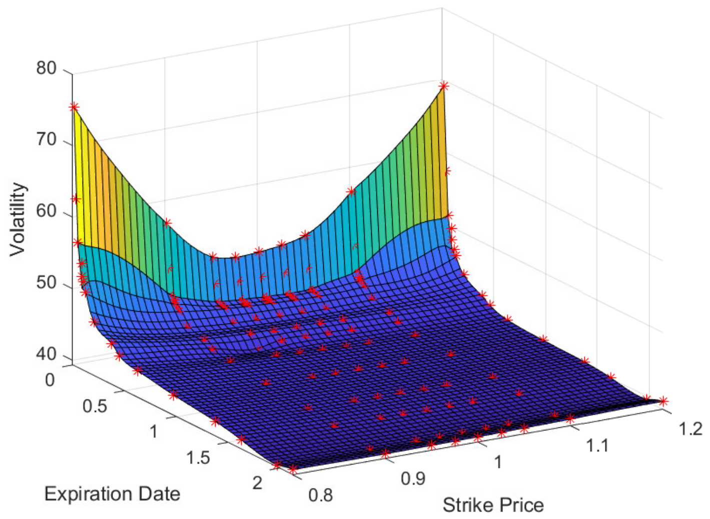

**Figure 2:** The surface obtained with the Thin Plate Spline.

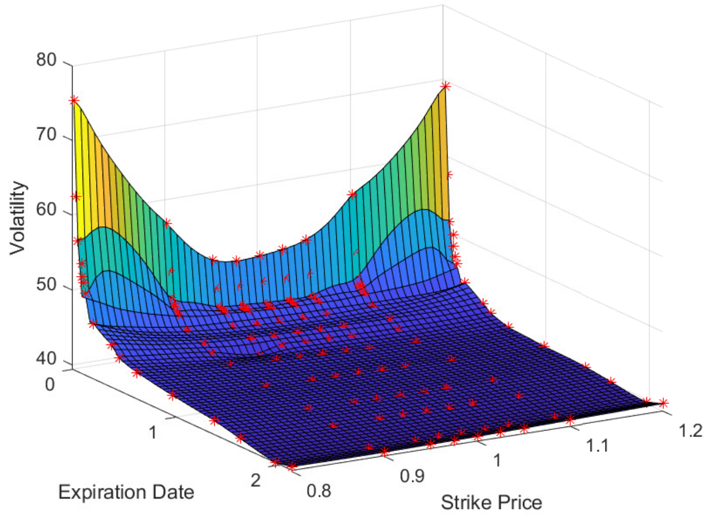

**Figure 3:** The surface obtained with Multiquadric using shape parameter $\epsilon = 110$.

Both surfaces are obtained with a grid of $n = 55$ intervals in each direction, and the Multiquadric one is obtained with a shape parameter of $\epsilon = 110$. As it is clear from the Figures, Multiquadric's surface is very similar to the one obtained using Thin Plate Spline: differences emerge only on the boundary of the domain, and further discrepancies occur in the steepest regions where the differences between the chosen base function become relevant. By decreasing the shape parameter, the importance of its choice becomes evident: for instance, if we analyze the surface obtained with Multiquadric it turns out that by decreasing $\epsilon$ the surface considerably worsens. In particular for values of shape parameter lower than $\epsilon = 70$, the surface starts to show swings that become bigger if the parameter decreases.

Other radial basis functions, for instance Gaussian, do not succeed in the reconstruction and it may be due to the peculiar distribution of the data-points. In the Gaussian's case, it is zero far from the function's center and with low density zones of points that does not allow this base function for the reconstruction of the empty regions.

At the end, global interpolants are tested by the cross validation technique: we remove points and we compare the new surface with the original one. The cross validation approach consists indeed in removing some nodes of the dataset and using them to check the errors committed. We considered two cases and the differences between the two new interpolants and the older ones are reported in Figure 4 and Figure 5, wherein both from the first figure to second a rotation is performed to consent a better view of the error surface.

On the left we have represented the points of the dataset used (red points) and the points removed (green points), while on the right the error surfaces obtained using the previous reconstructions are shown. Error results are quite limited in space. The associated root mean square errors, relative to the removed points, that we computed for the first interpolant is $RMSE = 0.0025$, and for the second one $RMSE = 0.0484$. These errors can be considered acceptable since most financial assets are traded at the second decimal digit.

| | RMSE | MAE |
|---|---|---|
| Case 1 (first figure) | 0.0025 | 0.0035 |
| Case 2 (second figure) | 0.0484 | 0.0514 |

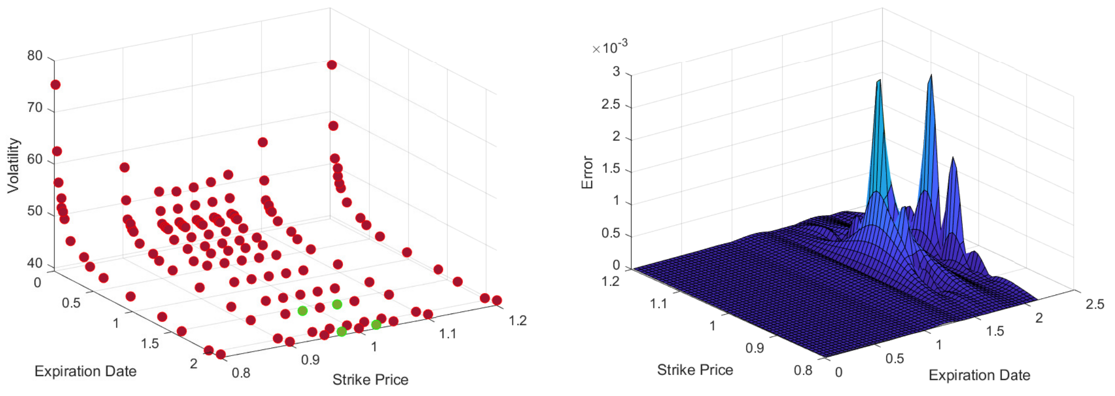

**Figure 4:** Plots show the first cross validation attempt (case 1): on the left the nodes of the dataset used (red points) and nodes removed (green points), on the right the plots of the errors.

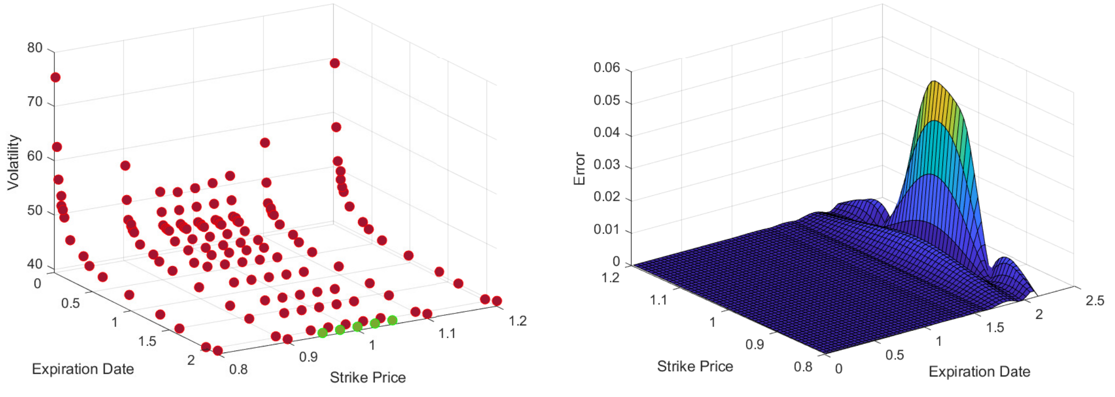

**Figure 5:** Plots show the second cross validation attempt (case 2): on the left the nodes of the dataset used (red points) and nodes removed (green points), on the right the plots of the errors.

## 3.2 Domain decomposition using RBFs

Following the dataset's characteristics and looking at how the surfaces fit it, we can easily recognize two different regions: the first is characterized by a steep decrease of implied volatility while the second one is flatter. Therefore, by using two interpolants instead of one, we could fit them in a better way splitting the dataset. Furthermore, studying the point's behavior, we can say that one possible way to split the dataset could be for the expiry date of 16/07/2021, when the behavior changes. Adopting this choice a first result is shown in the following figure.

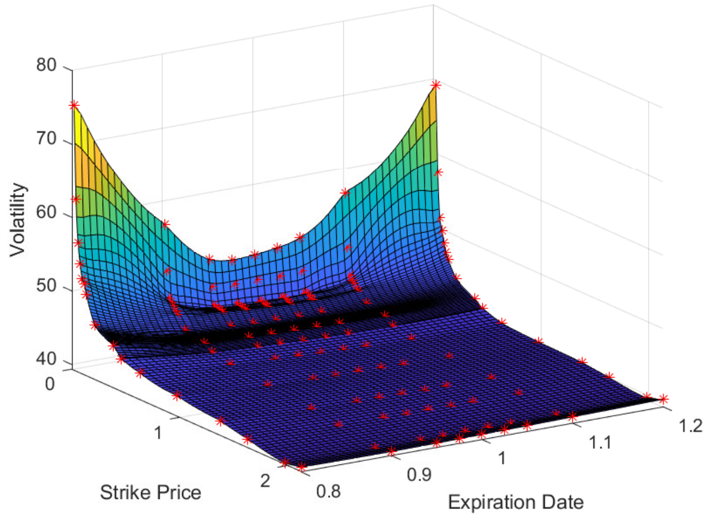

**Figure 6:** The surface obtained with splitting the dataset at 16/07/2021.

As expected the more local approach gives better results in terms of accuracy especially in those zones where the concentration of the points is greater, i.e. in the first part of the surface. This characteristic is more visible for maturities between 05/03/2021 (0.0958 in the chart) and 19/03/2021 (0.1342 in the chart) where, for strike prices near to the underlying value, the surface sharply flattens. Using this approach, we are able to capture these quick variations, allowing us to achieve a surface that fits our purpose well.

### 3.3 Numerical tests using PUM local interpolation

We try to produce surfaces that succeed to interpolate even better certain points as some boundary zones or those areas more steep. To achieve this result a local approach is taken using partition of unity method. This method is performed using a variable size of subdomains and shape parameters to find which of them better fit the dataset. Additionally, these tests are performed using normalization of the dataset to achieve better results. The first results are shown in Figure 7 and Figure 8.

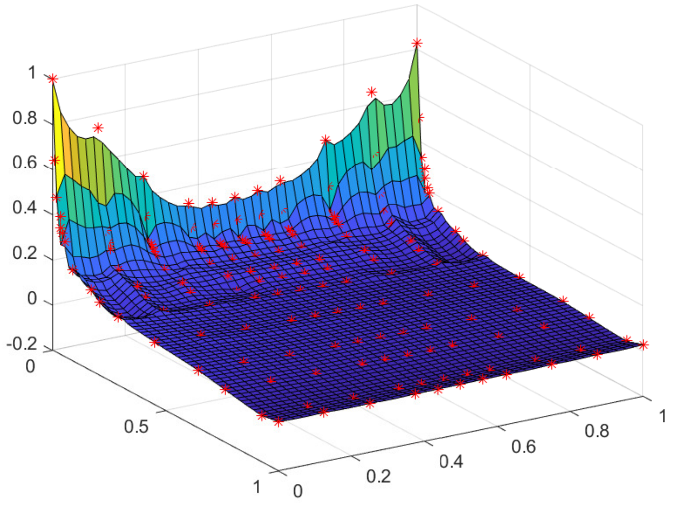

**Figure 7:** The surface obtained with the Thin Plate Spline-PUM.

The algorithm, for which more details can be found in [5], takes as input a vector of shape parameters and it automatically finds the best one. It is evident how the method performs in a different way based on zones and their quantity of points. In regions with more points, the partition of unity method performs better than the global method but it performs poorly in those

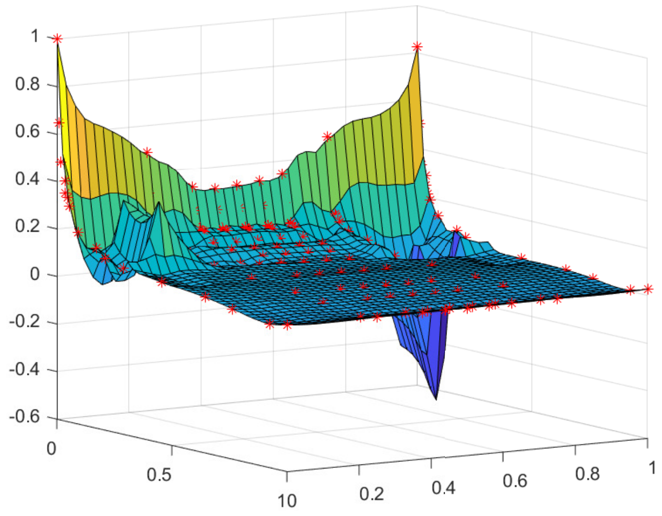

**Figure 8:** The surface obtained with Multiquadric-PUM.

zones with low density. This behavior can be linked to the local approach defined by the choice of the dimension (e.g. radius) of the subdomains.

To prevent a low level of surface accuracy we have decided to add points in the low-density data areas. To do so we added points obtained with the least square method: the approximation has been made along the time axis and from the obtained lines of points only four of them have been chosen on every row. Furthermore, a four degree polynomial is chosen to describe better the shape of so called volatility smile. Using that approach accuracy increases considerably, these improvements are visible in steepest zones where the combined choice of domain's radius and shape parameter is able to fit the points properly.
The results are presented in Figure 9, where a vector of 100 shape parameters equally spaced from $\epsilon = 50$ to $\epsilon = 200$ has been used.

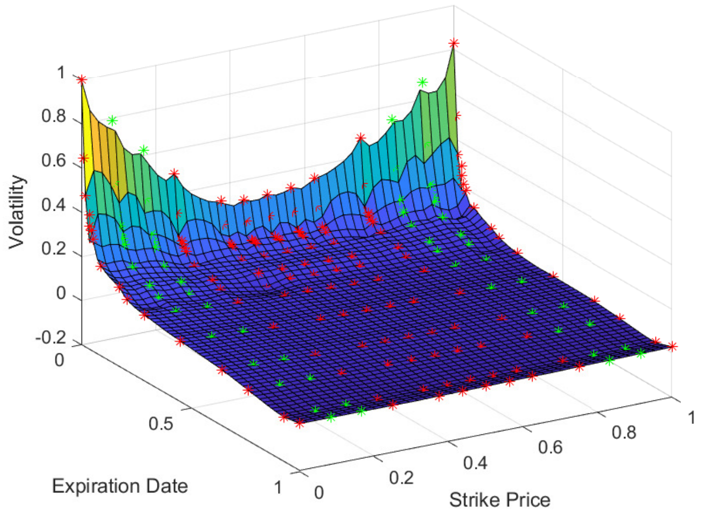

**Figure 9:** Surface obtained with PUM and Multiquadric. Initial points are colored by red while the newest ones computed using the least squares method are colored by green.

### 3.4 Numerical tests for surface extrapolation

Following studies are focused on extrapolating values of options' volatility for longer tenors and lower or higher strikes than the ones available in the market. To do so we try to extrapolate the obtained surfaces. At first we try to extrapolate from the date 17/03/2023 in order to find new points on date 29/12/2023. The extrapolation is shown in Figure 10.

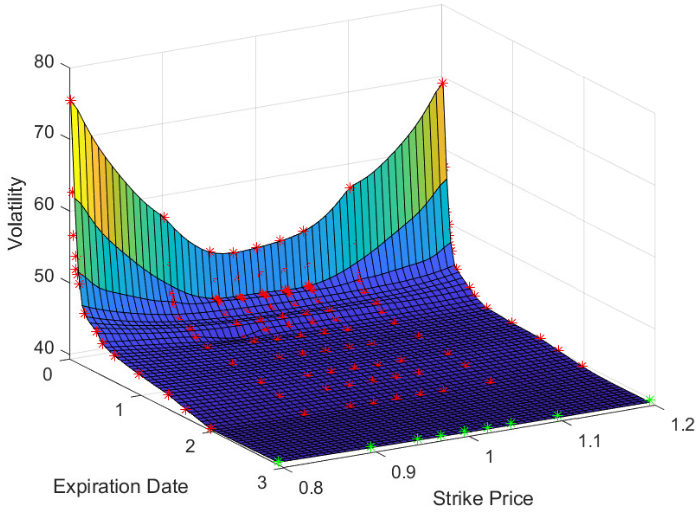

**Figure 10:** The figure above shows extrapolation obtained with multiquadric with shape parameter $\epsilon = 110$.

In Figure 10 we show Bloomberg points, reported in green. It has been observed that the maximum distance between our extrapolation and Bloomberg's data is of the order of 0.9%. Further investigation shows how our extrapolations diverge from Bloomberg's for more distant horizons. For instance, this maximum distance becomes 1.2% until 3.9 years (31/12/2024) and 2.1% until 4.9 years (31/12/2025). We can achieve better results by adopting the domain decomposition described above. Following this approach the maximum errors obtained diverge less than previous ones: for 2.9 years (29/12/2023), the distance became 0.89%, for 3.9 years (31/12/2024), the distance became 0.96% and finally for 4.9 years (31/12/2025) the distance became 1.76%. The predominant trend seems to be that Bloomberg's forecasts tend to be slightly more descent than ours. However since all these estimations are forecasts and not real data, we can consider the result promising.

## 4 Conclusions, remarks and future work

The efficiency and accuracy of the implied volatility surface interpolation problem have been investigated from a computational point of view. The radial basis function method and the partition of unity method implemented using RBFs as local approximants were considered. The best reconstruction results were obtained with RBFs, specifically using Thin plate Spline and Multiquadric, since the number of nodes involved was quite small. The RBF-PU interpolations deserve instead consideration when the number of nodes is large. Using the optimal selection of shape parameters and size of subdomains as presented in [5], can guarantee good approximations. Promising extrapolation results show that the topic needs further investigations. Work in progress concerns also the analysis of different datasets, in particular larger ones.

## Acknowledgements

This work was partially supported by the INdAM-GNCS 2020 research project "Multivariate approximation and functional equations for numerical modeling" and by the 2020 projects "Models and numerical methods in approximation, in applied sciences and in life sciences" and "Mathematical methods in computational sciences" funded by the Department of Mathematics "Giuseppe Peano" of the University of Torino. Moreover, this work was partially supported by the INdAM-GNCS 2020 research project "Interpolazione e smoothing: aspetti teorici, computazionali e applicativi". This research has been accomplished within the RITA (Research ITalian network on Approximation) and the UMI Group TAA (Teoria dell'Approssimazione e Applicazioni).

### References

[1] I. Babuška, J.M. Melenk, *The partition of unity method*, Internat. J. Numer. Methods. Engrg. 40 (1997), 727–758.

[2] F. Black, M. Scholes, *The Pricing of Options and Corporate Liabilities*, The Journal of Political Economy, vol. 81, 1973, pp. 637–654.

[3] M. D. Buhmann, *Radial basis functions: theory and implementation*, Cambridge Monogr. Appl. Comput. Math., vol. 12, Cambridge Univ. Press, Cambridge, 2003.

[4] R. Cavoretto, S. De Marchi, A. De Rossi, E. Perracchione, G. Santin, *Partition of unity interpolation using stable kernel-based techniques*, Appl. Num. Math. 116 (2017), pp. 95-107.

[5] R. Cavoretto, A. De Rossi, E. Perracchione, *Optimal Selection of Local Approximants in RBF-PU Interpolation*, J. Sci. Comput. 74 (2018), pp. 1–22.

[6] R. Cavoretto, A. De Rossi, *A two-stage adaptive scheme based on RBF collocation for solving elliptic PDEs*, Comput. Math. Appl. 79 (2020), 3206–3222.

[7] R. Cavoretto, A. De Rossi, *Error indicators and refinement strategies for solving Poisson problems through a RBF partition of unity collocation scheme*, Appl. Math. Comput. 369 (2020), 124824.

[8] R. Cavoretto, A. De Rossi, W. Erb, *Partition of unity methods for signal processing on graphs*, J. Fourier Anal. Appl. (2021) 27 (2021), 66.

[9] S. Cuomo, F. Piccialli, F. Sica, *RBF methods in a Stochastic Volatility framework for Greeks computation*, J. Comput. Appl. Math. 380 (2020), 112987.

[10] S. Cuomo, F. Sica, G. Toraldo, *Greeks computation in the option pricing problem by means of RBF-PU methods*, J. Comput. Appl. Math. 376 (2020), 112882.

[11] E. Derman, I. Kani, *Riding on a smile*, Risk Magazine, vol. 7, 1994, pp. 32–39.

[12] B. Dupire, *Pricing with a Smile*, Risk Magazine, vol. 7, 1994, pp. 18–20.

[13] B. Dupire, *A Unified Theory of Volatility*, Derivatives Pricing: The Classic Collection, Risk Books, 1996, pp. 185–196.

[14] G. E. Fasshauer, *Meshfree approximation methods with* Matlab, World Scientific, Singapore, 2007.

[15] G. E. Fasshauer, *Positive definite kernels: Past, present and future.*, Dolomites Research Notes on Approximation **4** (2011), pp. 21–63.

[16] G. E. Fasshauer, M. J. McCourt, *Kernel-based approximation methods using* Matlab, World Scientific, Singapore, 2015.

[17] M.R. Fengler, *Arbitrage-Free Smoothing of the Implied Volatility Surface*, SFB 649 Economic Risk, 2005.

[18] P.S. Hagan, D. Kumar et al., *Managing smile risk*, Risk Magazine, vol. 7, 1994, pp. 32–39.

[19] S.L. Heston, *A Closed-Form Solution for Options with Stochastic Volatility with Applications to Bond and Currency Options*, The Review of Financial Studies, vol. 6, 1993, pp. 327–343.

[20] A. Iske, *Scattered data approximation by positive definite kernel functions*, Rend. Sem. Mat. Univ. Pol. Torino, **69** (2011), pp. 217–246.

[21] J. M. Melenk, I. Babuška, *The partition of unity finite element method: basic theory and applications*, Comput. Methods. Appl. Mech. Engrg. 139 (1996), 289–314.

[22] A. Safdari-Vaighani, A. Heryudono, E. Larsson, *A radial basis function partition of unity collocation method for convection-diffusion equations arising in financial applications*, J. Sci. Comput. **64** (2015), pp. 341–367.

[23] R. Schaback, *Error estimates and condition numbers for radial basis function interpolation*, Adv. Comput. Math. **3** (1995), 251–264.

[24] V. Shcherbakov, E. Larsson *Radial basis function partition of unity methods for pricing vanilla basket options*, Comput. Math. Appl. 71 (2016), 185–200.

[25] L. von Sydow, S. Milovanović, E. Larsson, K. In't Hout, M. Wiktorsson, C. W. Oosterlee, V. Shcherbakov, M. Wyns, A. Leitao, S. Jain, T. Haentjens, J. Waldén, *BENCHOP - SLV: the BENCHmarking project in Option Pricing - Stochastic and Local Volatility problems*, Int. J. Comp. Math. 96 (2019), 1910–1923.

[26] H. Wendland, *Fast evaluation of radial basis functions: methods based on partition of unity*, in Approximation Theory X: Wavelets, Splines, and Applications, C. K. Chui, L. L. Schumaker, J. Stöckler, eds., Vanderbilt Univ. Press, Nashville, TN, 2002, pp. 473–483.

[27] H. Wendland, *Scattered data approximation*, Cambridge Monogr. Appl. Comput. Math., vol. 17, Cambridge Univ. Press, Cambridge, 2005.